

Analysis of the electrochemical phenomenon at the rebar–concrete interface using the electrochemical impedance spectroscopic technique

R. Vedalakshmi and N. Palaniswamy

Central Electrochemical Research Institute

The corrosion rate of rebar during the various stages where it occurs, such as passivation, initiation of corrosion and severe corrosion, needs to be determined non-destructively for the maintenance, restoration and replacement of concrete structures. The double layer capacitance (C_{dl}) and the charge transfer resistance or polarisation resistance (R_p) of the corrosion processes have been associated with the slope of the low-frequency arc in the Nyquist plot, and this can be related to the electrochemical phenomenon that occurs at the steel–concrete interface. The present studies, based on electrochemical impedance spectroscopy (EIS) conducted on three different densities of concrete with addition of 0.5 and 1% chloride over a period of 1765 days, reveal that the capacitive behaviour of a low-frequency arc with a slope more than -1 indicates the passive condition of rebar. Warburg diffusion behaviour with a slope exactly equal to -1 denotes the initiation of corrosion on the rebar. A slope of less than -1 is obtained when corrosion spreads uniformly on the rebar. Other electrochemical parameters such as R_p , C_{dl} and phase angle are correlated with the phenomenon occurring at the steel–concrete interface. An R_p value greater than $250 \text{ k}\Omega \text{ cm}^2$ indicates the passive condition of rebar, whereas values of less than 230 and $14 \text{ k}\Omega \text{ cm}^2$ indicate initiation and severe corrosion of the rebar respectively. Similarly, a C_{dl} value greater than $1000 \mu\text{F}/\text{cm}^2$ indicates the severe corrosion of rebar, whereas less than $100 \mu\text{F}/\text{cm}^2$ denotes the passive condition of rebar. If the rebar is in the passive condition, the phase angle is more than 30° , whereas it is less than 20° under severe corrosion. The reduction of intrinsic chloride diffusivity owing to pore restructuring by pozzolanic reaction and adsorption of a greater amount of chloride ions into the interlayer of additional calcium silicate hydrate content are responsible for delayed initiation of corrosion in Portland pozzolana cement (PPC) and Portland slag cement (PSC) concretes, when compared with ordinary Portland cement (OPC) concrete.

Introduction

Reinforced concrete is a composite material made of an active metal, namely rebar, and a non-metallic material – that is, concrete. Concrete behaves like an unpredictable electrolyte and the rebar encased by it is inaccessible during service. Periodic inspection is necessary, especially for structures in highly aggressive environments, as a risk-prevention strategy. The passive/

active condition of rebar is determined using potential and resistivity measurements non-destructively. The threshold potential value of -276 mV versus saturated calomel electrode (SCE) as specified in ASTM C876 (ASTM, 2001a) is taken as initiation of corrosion and this criterion is widely used both in laboratory and field conditions because it is simple and well established. The presence of moisture, oxygen availability and the resistance of the cover concrete all influence the measured potential values, which are different from the actual values. Sometimes this can be misleading when interpreting the results, particularly when the concrete is under very dry or wet conditions. Arup (1983) reported that variations of potential values are so broad that confusion between the passive and active states would be

Corrosion Protection Division, Central Electrochemical Research Institute, Karaikudi, 630 006, Tamil Nadu, India

(MACR 800165) Paper received 12 September 2008; last revised 14 June 2009; accepted 3 September 2009

possible in many situations. For example, when the rebar is under the passive state, the potential may vary from +200 mV to -700 mV versus SCE, while in concrete with limited oxygen access, the potential can be shifted to around -1000 mV versus SCE. Permanently installed embeddable reference electrodes such as manganese dioxide (MnO_2), silver/silver chloride (Ag/AgCl), mercury/mercury (II) oxide (Hg/HgO) etc., kept close to the reinforcement eliminate the difficulties described above (Arup and Sorenson, 1992; Bennett and Amitchell, 1992; Dolli *et al.*, 2003; Vilella *et al.*, 2004). The stability of these reference electrodes is questionable, however, as they are affected by changes in moisture, oxygen, chloride level and pH of the concrete more directly and it is reported that the drifts may be up to 60 mV (Videm, 1998). Surface potential measurements using two reference electrodes are also used for non-destructive testing to identify anodic and cathodic regions in a concrete structure and, indirectly, to detect the corrosion of rebar qualitatively (Florr and Keith, 1965; Rengaswamy *et al.*, 1987; Stratfull, 1957). It is generally accepted that the potential measurements must be supplemented using other methods as well.

During any corrosion process, the corrosion current has to flow from the site of the anode to the cathode through the electrolyte and the resistivity of the concrete has an influence on the flow of this current. Higher electrical resistance can impede the flow of such currents and hence, depending upon the resistivity of the concrete, the corrosion process can be stifled or accelerated. Some researchers (Gonzalez *et al.*, 2004; Morris *et al.*, 2002) have correlated the resistivity of the concrete with the corrosion current (i_{corr}) qualitatively. If the resistivity of the concrete is greater than 100 k Ω cm then there will be only negligible i_{corr} , but if the resistivity is less than 20 k Ω cm then there will be very high i_{corr} , which leads to cracking of cover concrete (Andrade *et al.*, 1993; Gonzalez *et al.*, 2004; Grimes *et al.*, 1979). When using these criteria, the variations in the wetness of the concrete are much greater, and therefore the variations in the resistivity values can differ by a factor of 4. Both the potential and resistivity measurements give only qualitative data on the status of the rebar.

The quantitative measurement of i_{corr} of the rebar based on the linear polarisation resistance (LPR) method is the best complementary electrochemical technique used by various researchers (Andrade *et al.*, 2002; Bulu and Bhattacharjee, 2009; Feliu *et al.*, 1989; Flis *et al.*, 1993; Grantham and Broomfield, 1997; Lawa *et al.*, 2004; Zivica, 2001). If quantitative data have to be obtained then it is necessary to polarise the steel rebar. The polarisation is influenced to a greater or lesser degree by the presence of diffusion polarisation. The LPR method cannot separate the contributions of the various electrochemical processes involved, such as charge transfer resistance, concentration polarisation, interfacial layers or ohmic resistance

of the concrete. Additionally, in the experimental methods, for example in the potentiodynamic method, the large and unpredictable pseudo capacitance of the steel in concrete causes a charging current that overshadows the Faraday current. On the other hand, if the LPR measurement is carried out using the potentiostatic method, a longer waiting period leads to a current that decreases with time, so that, in turn, R_p is dependent on the test time. None of the above methods can predict the electrochemical phenomenon that occurs at the steel-concrete interface accurately. Thus any measurement technique should take into account the inaccessibility of the steel and the space/time variations that occur at the rebar-concrete interface.

Electrochemical impedance spectroscopy (EIS), which involves measurement in the frequency domain, is a well-established technique for the identification of interfacial effects involved in the transfer of charge together with the detection of diffusional and electrolyte impedances (Andrade *et al.*, 1999; Ismail and Ohtsu, 2006; John *et al.*, 1981; Montemor *et al.*, 2000; Monticelli *et al.*, 2000; Wenger and Galland, 1990). The impedance plots contain several time constants. Often portions of one or more semicircles are obtained, depending on the number of time constants involved in the kinetics of the corrosion processes. For example, if the steel in the concrete is strongly influenced by the chloride concentration gradient, the concentration effects can be easily distinguished by the presence of Warburg impedance. Dispersion of the time constant causing depression of the semicircle in the Nyquist plot indicates the presence of a constant phase element. Hence each time constant occurring at the steel-concrete interface is indicated by the presence of a well-defined curve in the Nyquist plot. With all the above advantages, the use of small signals (10–20 mV) in the EIS technique causes minimum disturbance to the rebar surface and can measure the corrosion rate in low-conductivity media such as concrete, whereas direct current (d.c.) techniques are affected by a number of errors.

The objective of the present study is to use the EIS technique to analyse the occurrence of passivation, initiation and uniform severe corrosion in the presence and absence of chloride. The possibility of using the R_p value to assess the time to initiation of corrosion is explored. In addition to this, the effect of reaction occurring at the rebar-concrete interface on various other electrochemical parameters such as ' α ' values, double layer capacitance and phase angle is also discussed.

Experimental method

Materials and mix proportions

Three mix proportions of concrete with a design compressive strength of 20, 30 and 40 MPa at 28 days

were used for casting the concrete specimens. The details of mix proportions are given in Table 1. The mix proportions were kept constant for both blended cement concrete and Portland cement concrete. Three cements were used, namely ordinary Portland cement (OPC) conforming to Bureau of Indian Standards BIS 8112 (BIS, 1989a) and equivalent to ASTM type I cement, Portland pozzolana cement (PPC) conforming to BIS 1489, Part 1 (BIS, 1991) and Portland slag cement (PSC) conforming to BIS 455 (BIS, 1989b). The chemical compositions of the cements used are presented in Table 2. Well-graded river sand and good-quality crushed blue granite were used as fine and coarse aggregates respectively. The different size fractions of coarse aggregate (20 mm downgraded and 12.5 mm downgraded) were taken and recombined to a specified grading. Cold twisted high-yield strength deformed bar (Fe-415 grade) conforming to BIS 1786 (BIS, 1985), with a diameter of 16 mm was used and its chemical

composition was carbon (C) 0.17%; manganese (Mn) 0.66%; silicon (Si) 0.115%; sulfur (S) 0.017%; phosphorus (P) 0.031; and iron (Fe) balance. Potable water was used for casting the concrete specimens.

Specimen preparation

150 × 150 × 150 mm sized concrete cubes as shown in Figure 1 were cast. Cold twisted deformed (CTD) rods 100 mm long and 16 mm in diameter were taken and pickled in inhibited hydrochloric acid solution to remove the initial rust product. In each specimen, three rods of similar dimensions were embedded at 25 mm cover from one side of the specimen. For electrochemical measurement, copper wire was brazed at one end of a particular rod and that was sealed. Impedance measurement was carried out over an exposed length of 8 cm and the remaining area was sealed using epoxy compound. For determining the corrosion rate from the weight loss measurement, another two rods were

Table 1. Details of concrete mix proportions

Grade	Type of cement	w/c ratio	Cement: kg/m ³	Water: kg/m ³	Fine aggregate: kg/m ³	Coarse aggregate: kg/m ³	Characteristic compressive strength: MPa
20 MPa	OPC	0.67	284	190	770	1026	27
	PPC	0.67	284	190	770	1026	23
	PSC	0.67	284	190	770	1026	28
30 MPa	OPC	0.54	352	190	739	1026	37
	PPC	0.54	352	190	739	1026	31
	PSC	0.54	352	190	739	1026	39
40 MPa	OPC	0.42	452	190	655	1026	54
	PPC	0.42	452	190	655	1026	42
	PSC	0.42	452	190	655	1026	48

Table 2. Chemical composition and physical properties of the three types of cement

	Ordinary Portland cement: %	Portland pozzolana cement: %	Portland slag cement: %
<i>Compound</i>			
Silicon dioxide (SiO ₂)	20–21	28–32	26–30
Aluminium oxide (Al ₂ O ₃)	5.2–5.6	7.0–10.0	9.0–11.0
Ferric oxide (Fe ₂ O ₃)	4.4–4.8	4.9–6.0	2.5–3.0
Calcium oxide (CaO)	62–63	41–43	44–46
Magnesium oxide (MgO)	0.5–0.7	1.0–2.0	3.5–4.0
Sulfur trioxide (SO ₃)	2.4–2.8	2.4–2.8	2.4–2.8
Loss on ignition	1.5–2.5	3.0–3.5	1.5–2.5
<i>Bogue compound composition:</i>			
Tricalcium silicate (C ₃ S)	42–45	Not applicable	Not applicable
Dicalcium silicate (C ₂ S)	20–30	Not applicable	Not applicable
Tricalcium aluminate (C ₃ A)	7.0–9.0	Not applicable	Not applicable
Tetra calcium aluminoferrite (C ₄ AF)	11–13	Not applicable	Not applicable
<i>Physical properties</i>			
Pozzolan material used: %	–	Around 20% fly ash (Mettur thermal power station)	Around 50% GGBS (Vizag steel plant)
28-day compressive strength: MPa	62	48	53
Fineness: m ² /kg	295	363	385

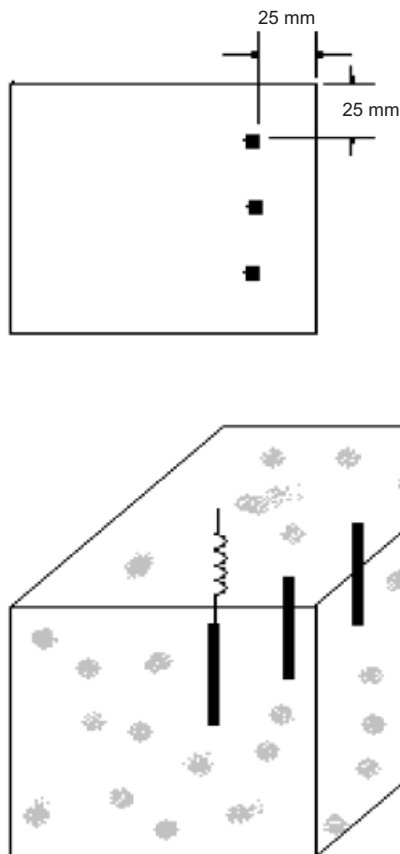


Figure 1. Rebar arrangements in a concrete specimen

embedded near the previous one, as shown in Figure 1. Before embedding, the initial weight of the rods was recorded. In one set of specimens, no chloride (0%) was added to the concrete and in another set of specimens, 0.5% and 1% of sodium chloride by weight of cement was added at the time of casting. While casting, all the three rebars were embedded vertically with a 25 mm cover from the top and bottom. Four specimens were cast for each grade/cement. All of the specimens were cured at room temperature for 28 days in potable water.

Exposure condition

After 28 days of curing, the specimens were exposed in the exposure yard. Synthetic seawater was prepared as specified in ASTM D-1141-98 (ASTM, 2001b). Synthetic seawater was sprayed horizontally using a spray gun once per day for five days on one side of the specimen and then the specimen was air dried for the next two days. Thus seven days constituted one cycle of wetting and drying. All the specimens were subjected to similar exposure conditions. This test procedure simulates the atmospheric exposure of concrete structures in a marine environment. The temperature, relative humidity and other parameters prevailing at the exposure site are given in Table 3. As the exposure site is situated more than 2.5 km from the sea, the atmospheric salinity at the exposure site is lower than at the

Table 3. Meteorological data

	Max.	Min.
Temperature (average): °C	33	21
Relative humidity (average)	80	65
Rainfall (average): mm	180	
SO ₂	Nil	
Salinity: mg/m ² day	38	

coast, so it was necessary to resort to periodic salt spray. The experiment was conducted over a period of 1765 days. Periodically, the concrete specimens were broken open and the rods were visually examined for the extent of rust. After pickling the rebars in inhibited hydrochloric acid as specified in ASTM G1-03 (ASTM, 2001c), the final weight was measured. From the initial and final weight, the corrosion rate in $\mu\text{m}/\text{year}$ was calculated as

$$\text{Corrosion rate in } \mu\text{m}/\text{year} = \frac{87\,600w}{DAT} \quad (1)$$

where w is the loss in weight (mg); D is the density of iron (g/cm^3); A is the area (cm^2); and T is time (h).

Method of measurement

Polarisation resistance. The potential of the rebar was measured periodically using a high-input impedance multimeter. A saturated calomel electrode was used as the reference electrode. Impedance measurement was made using three electrode arrangements. A stainless steel electrode of size 10 mm \times 80 mm was used as an auxiliary electrode and the saturated calomel electrode was used as the reference electrode. Rebar embedded in concrete acted as a working electrode. The electrode assembly was kept on a wetted sponge. The length of the counter electrode is more than the exposed length of the rebar and, by means of this, current was distributed uniformly throughout the length of the rebar. Chloride solution was used as a contacting solution to reduce the contact resistance between the electrode assembly and the concrete. A small sinusoidal voltage signal of 20 mV was applied over a frequency range of 100 kHz to 10 mHz using a computer-controlled electrochemical analyser (Model 6310 from E G & G Instruments, Princeton Applied Research). Measurements were made periodically at the end of 80, 267, 540, 1135 and 1765 days. The impedance values were plotted on the Nyquist plot. From the Nyquist plot, using the software 'z view', the concrete resistance (R_c) and polarisation resistance (R_p) were determined by extrapolating the high-frequency arc (100 kHz–100 Hz) and the low-frequency arc (100 Hz–10 mHz) respectively. From the Bode plot, the phase angle at the frequency of 10 mHz was recorded.

Calculation of α values and double layer capacitance (C_{dl})

In EIS experiments, the capacitors often do not behave ideally. Instead, they act like a constant phase element (CPE), as shown in an equivalent circuit presented in Figure 2. The impedance of a capacitor has the form

$$Z_{CPE} = \frac{1}{C(j\omega)^\alpha} \quad (2)$$

where C is the capacitance and α is the exponent for CPE impedance due to the depressed semicircle. For a CPE the exponent α is less than 1. The double layer capacitance on the real axis often behaves like a CPE. A clockwise rotation of the ideal semicircle in the Nyquist plots over an angle $(1 - \alpha) \pi/2$ suggests the action of CPE. This is shown in Figure 3. From the depression angle, the α value was calculated. According to the literature (Bohnke *et al.*, 1993; Rammelt and Reinhard, 1995) the charging of a discontinuous and inhomogeneous interface leads to a CPE-like response. A response of this type in the steel–concrete system is therefore to be expected both as a result of the lack of

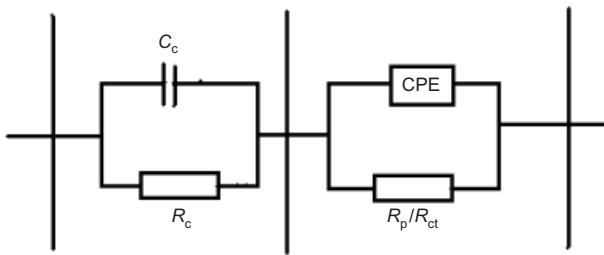


Figure 2. Equivalent circuit of rebar in the passive state

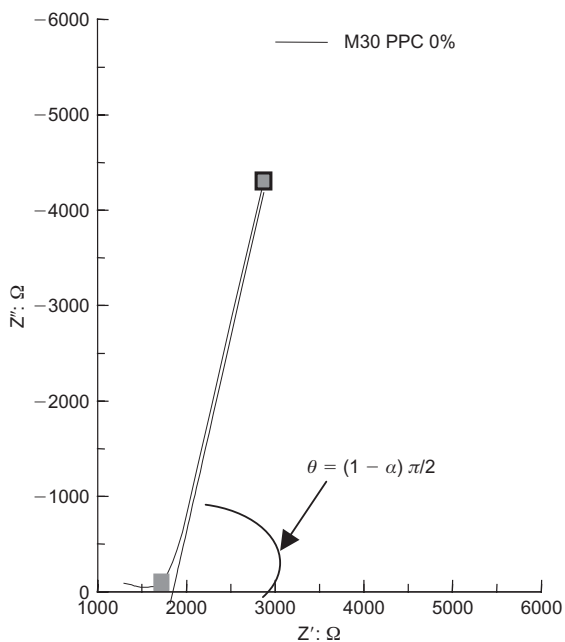


Figure 3. Impedance behaviour of the CPE

surface homogeneity of the rebar (e.g. surface roughness and distribution of isolated reaction zones) and of the eminently heterogeneous nature of the concrete. Hence, in the equivalent circuit as shown in Figure 2, the CPE has been introduced. The CPE may be viewed as resembling a capacitor–resistor series combination in which both components have frequency-dependent values. With the introduction of a CPE as a replacement for the capacitor in EIS measurements, the C_{dl} values obtained from the Nyquist plot have been corrected using the following formula (Jovic and Jovic, 2003)

$$C_{dl} = A_{dl}(\omega'_{max})^{\alpha-1} \quad (3)$$

where ω'_{max} represents the frequency of the maximum on the $-Z''$ against ω dependence, which is independent of the exponent α , whereas A_{dl} represents the result of fitting of the Nyquist plot.

Results

Slope of the low-frequency arc

Passive condition of the rebar. Invariably in all the Nyquist plots obtained (Figure 4, and later Figures 6 and 8) two arcs are present. One at the high-frequency region (100 kHz–100 Hz) and another one at the low-frequency region (100 Hz–10 mHz). A frequency above 1 Hz reflected mainly the conductance properties of the concrete and was hardly influenced by the charge transfer resistance of the rebar. Hence the changes occurring at the steel–concrete interface can be easily distinguished from the changes in the low-frequency curve. By extrapolating the low-frequency curve as a straight line to the real axis, the slope of the curve was obtained.

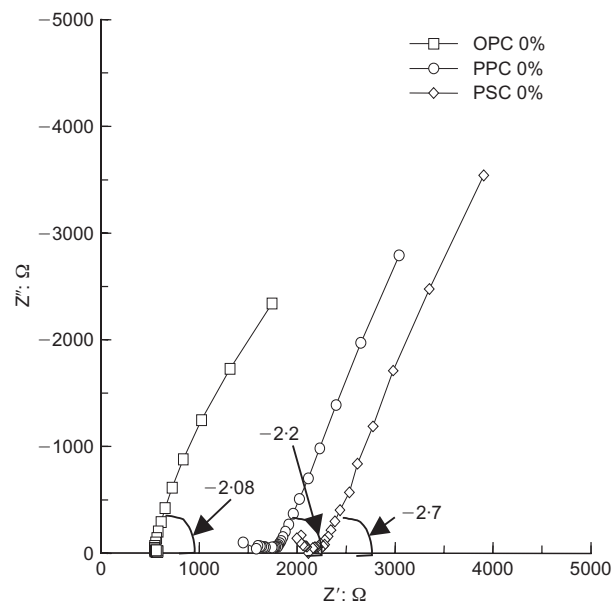


Figure 4. Nyquist plot of rebar in the passive state in 40 MPa concrete (80 days)

From Table 4, it can be seen that initially when the rebar is in the passive condition – that is, up to the period of 80 days – the slope of the low-frequency arc varies from -0.72 to -3.72 . Due to the presence of large and non-ideal apparent interfacial capacitance at the steel–concrete interface, surface inhomogeneity on the rebar (ribbed bar) and the heterogeneous nature of concrete, the double layer capacitance of rebar behaves like a constant phase element (CPE) instead of like a pure capacitor (Sagues *et al.*, 1995). From Table 4, it can be seen that at the end of 80 days, in almost all the cases except M20-OPC 1% Cl^- added concrete, the slope of the curve is greater than -1 and confirmed the presence of the CPE. From the analysis, the assumed equivalent circuit is given in Figure 2 and the corresponding Nyquist plot is given in Figure 4. From the figure, it can be seen that the slope of the low-frequency arc in the frequency range 3 Hz–10 mHz is -2.08 , -2.2 and -2.7 in M40 OPC, PPC and PSC concrete respectively. This represents the non-ideal capacitance behaviour of rebar in 40 MPa concrete when the rebar is under the perfect passive condition. A higher slope indicates that the passivation of the rebar is higher. Compared with 20 MPa concrete, in 30 and 40 MPa concretes, the values are higher. Due to the higher cement content and the reduced water-to-cement (w/c) ratio in 30 and 40 MPa concretes, the availability of alkalinity at the steel–concrete interface is higher and the chloride is lower, thus complete passivity is established. Pruckner (2001) reported that the hydroxide (OH^-) ions concentration in the pore solution varied from 158.5 mM/l to 501.20 mM/l if the w/c ratio was varied from 0.7 to 0.4. The passive behaviour of rebar in these concretes is not changed up to the presence of 1% chloride near the rebar. The high alkalinity of cement paste offers satisfactory protection against corrosion owing to the existence of a self-generating protective layer γ -ferric oxide ($\gamma\text{-Fe}_2\text{O}_3$) at the steel–concrete interface. This protective layer occurs during

the initial stages of cement hydration and grows with time up to 80 days. As reported in the literature, the passive layer grows to a thickness of the order of 10^{-3} – 10^{-1} μm and is rich in lime content (Sagoe-Crentsil and Glasser, 1989). This adherent surface film maintains the perfect passive condition in the presence of up to 1% of added chloride.

Active condition of the rebar. The diffusion of chloride means that the rebar attains an active state and in this state two conditions are possible: one is when the chloride ions reach the threshold value and they break the passive film, when corrosion initiates on the rebar; the other is that, with time, corrosion spreads uniformly throughout the rebar surface. At the initiation of corrosion, the rebar is under mixed kinetic and diffusion-controlled reaction, and Warburg impedance (WI) is possible, whereas at uniform corrosion only the corrosion process is possible. The assumed equivalent circuits and the corresponding Nyquist plots for the above two conditions are given in Figures 5 and 6 and Figures 7 and 8 respectively.

In Figure 6 it can be observed that, when compared with Figure 4, the slope of the curve slowly decreases

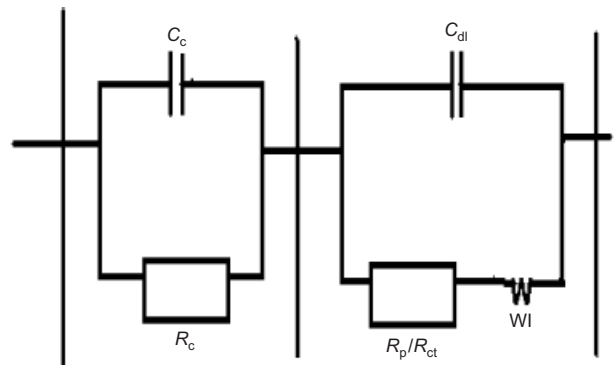


Figure 5. Equivalent circuit of rebar under initiation of corrosion

Table 4. Comparison of slope of the low-frequency curve

Grade/type of cement	Exposure period								
	80 days (passive condition)			540 days (initiation of corrosion)			1135 days (severe corrosion)		
	% of chloride								
	0	0.5	1	0	0.5	1	0	0.5	1
20 MPa OPC	-0.72	-0.29	-1.02	-0.28	0.21	-0.12	-0.23	0.21	-0.28
20 MPa PPC	-1.18	-2.54	-1.50	-1.27	-0.67	-0.25	-0.63	-0.19	-0.39
20 MPa PSC	-1.58	-0.45	-0.71	-2.02	-0.39	-0.73	-0.23	-0.17	-0.27
30 MPa OPC	-1.18	-1.34	-2.73	-0.12	-0.30	-0.24	-0.45	-0.62	-0.15
30 MPa PPC	-3.72	-1.97	-1.54	-1.10	-1.03	-1.41	-1.96	-0.60	-0.76
30 MPa PSC	-2.57	-2.96	-2.41	-2.54	-1.28	-1.43	-1.18	-1.51	-0.41
40 MPa OPC	-2.08	-1.60	-2.84	-0.63	-2.74	-1.57	-0.13	-1.18	-0.27
40 MPa PPC	-2.20	-2.54	-1.22	-1.31	-1.60	-0.85	-1.42	-0.81	-0.66
40 MPa PSC	-3.20	-2.72	-1.83	-2.63	-1.69	-1.25	-	-0.92	-1.02

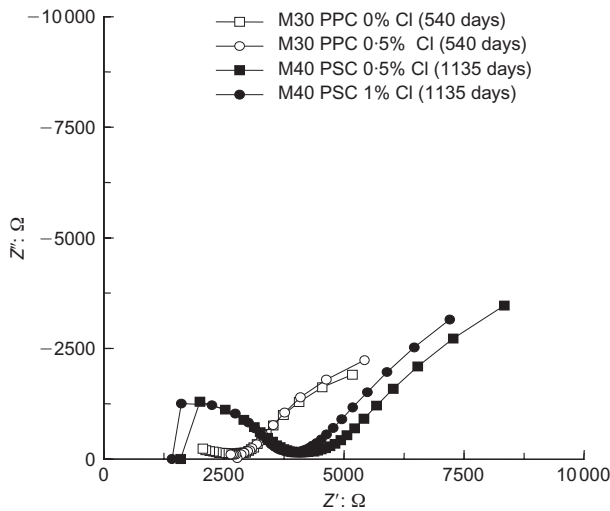


Figure 6. Nyquist plot of rebar under initiation of corrosion

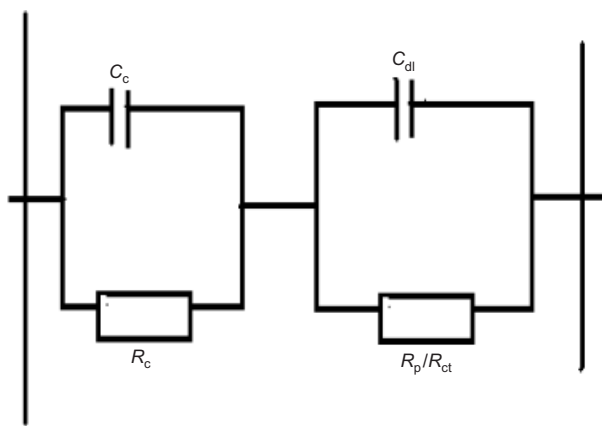


Figure 7. Equivalent circuit of rebar under uniform corrosion

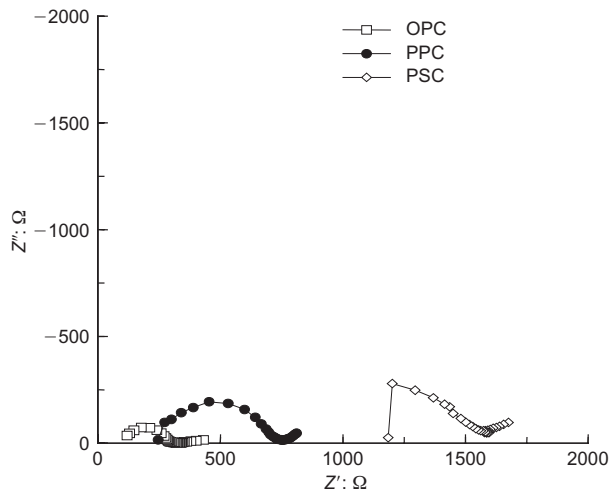


Figure 8. Nyquist plot of rebar under uniform corrosion (1135 days)

with time. If corrosion is initiated on the rebar, the slope of the low-frequency arc in the Nyquist plot reaches -1 and indicates the presence of Warburg impedance. The initiation of corrosion depends on the

rate of diffusion of chloride. From Table 4, it can be observed that after 540 days of exposure, in 30 and 40 MPa concretes for most of the cases the values are -1 , whereas in 20 MPa concrete the values are less than -1 . Compared to 30 and 40 MPa concrete, in 20 MPa concrete, the rate of diffusion of chloride is greater, corrosion spreads over a larger area and decreases the slope value to less than -1 .

With time, if corrosion spreads throughout the rebar uniformly, then the slope of the curve decreases further and reaches less than -1 , as shown in Figure 8. The slope at the end of 1135 days (active condition) is compared in Table 4. From the table it can be seen that the slope of the curve embedded in 20 MPa 0% Cl^- added concrete as given in Figure 8 is -0.23 , -0.63 and -0.23 in OPC, PPC and PSC concretes respectively. It is evident that the slope is less than -1 and indicates that the reaction is a Faradaic corrosion process with the rate depending on the mass transfer control. Hence the assumed equivalent circuit as given in Figure 6 consists of R_p and C_{dl} only. Due to the reduced rate of corrosion, the slope is higher in 30 and 40 MPa concretes compared with that of 20 MPa concrete. Compared to OPC concrete, the slope values are higher in PPC and PSC concretes. Reduced rate of diffusion of chloride due to the densification of pore structure by the pozzolanic reaction and the higher chloride binding ability are contributing to the reduction of corrosion rate of PPC and PSC concretes. Similarly, Montemor *et al.* (2000) also reported that the slope of the curve obtained in the Bode plot seems to reflect the charge transfer resistance of the rebar and it was not affected by the resistance of the concrete.

α values. Figures 9(a), (b) and (c) compare the variation of α values in 20, 30 and 40 MPa concrete. From the figures it can be seen that up to the period of 80 days, when the rebar is in the passive condition, the α values vary from 0.7 to 0.85, which are of the same order as those found by Sagues *et al.* (1995) for steel in concrete. Compared to OPC concrete, the α values are higher in PPC and PSC concretes in all the three strengths of concrete. Up to 540 days, in the presence of 1% of chloride, the α values are higher in 30 and 40 MPa concrete than in 20 MPa concrete. After 540 days of exposure in 30 and 40 MPa with 1% chloride added concrete, the α values are decreased and found to be in the range 0.67–0.24, whereas in the case of 20 MPa OPC concrete, the values are less than 0.67 right from the initial stage onwards. The rust product formed on the rebar surface increases the surface roughness and this might have decreased the α values.

Double layer capacitance (C_{dl})

In the Nyquist plot, R_p and C_{dl} are a pair of ‘measured’ values obtained throughout the fitting process and they have overall effects on the rebar surface corrosion

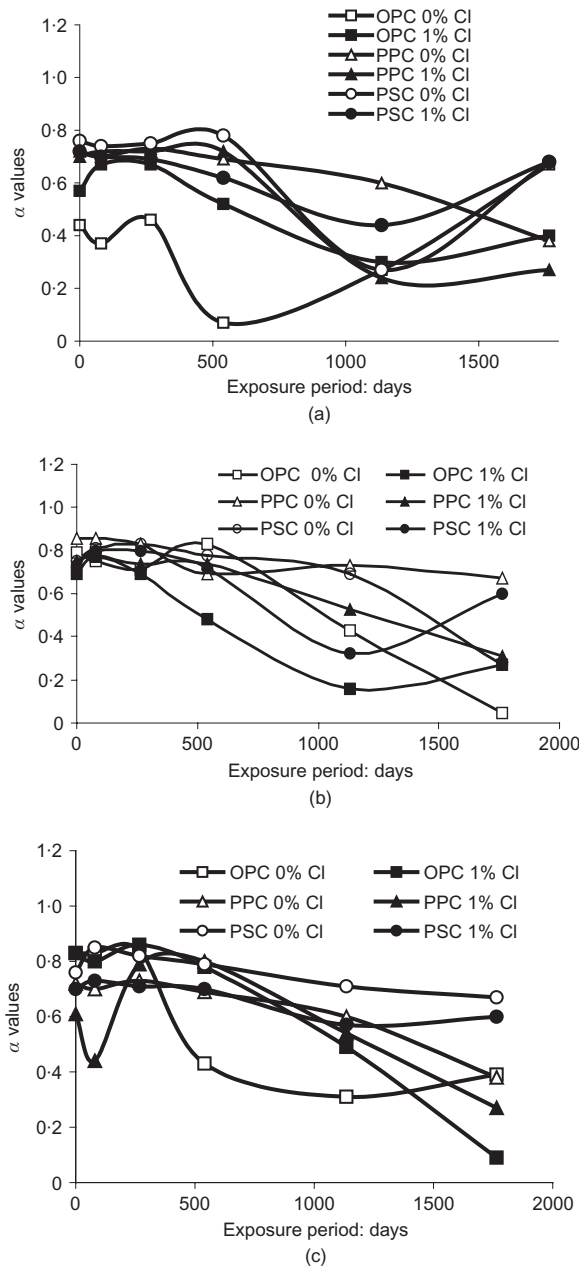


Figure 9. Variation of α values with time: (a) in 20 MPa concrete; (b) in 30 MPa concrete; (c) in 40 MPa concrete

kinetics. The C_{dl} value here is an overall capacitance containing a double layer capacitance and a pseudo-capacitance associated with adsorption of species such as chloride, oxygen and hydroxyl ions on the rebar surface. In the present study this has been related qualitatively to the adsorption/desorption of chloride at the steel–concrete interface. As the concrete specimens were exposed under a chloride environment, chloride is the only aggressive ion responsible for the rate of activation of the corrosion process. If the C_{dl} value is less than $500 \mu\text{F}/\text{cm}^2$, then adsorption of chloride ions is less and the rebar is able to maintain its passive condition. If the C_{dl} value is greater than $500 \mu\text{F}/\text{cm}^2$ then this indicates that the rebar is in the active condition. Similarly Gu *et al.* (1997) reported that the C_{dl} value of rebar embedded in 0% Cl^- added concrete was $78.5 \mu\text{F}/\text{cm}^2$ and increased to $1988 \mu\text{F}/\text{cm}^2$ in 4% Cl^- added concrete. The corrected C_{dl} values after introducing the CPE using Equation 3 are given in Tables 5 and 6.

Passive condition of the rebar. Table 5 compares the C_{dl} value with time in 40 MPa concrete up to the period of 540 days. In 40 MPa concrete, in most of the cases the C_{dl} values are less than $500 \mu\text{F}/\text{cm}^2$. The data emphasise that the smaller amount of adsorption of free chloride ions at the steel–concrete interface owing to higher chloride binding ability of PPC and PSC concrete reduced the C_{dl} values compared with that of OPC concrete. In addition, the formation of additional calcium hydrates in blended cement concretes may provide certain inhibitive effects on the rebar (Glass and Buenfield, 1999; Glass *et al.*, 2000; Sergi and Glass, 2000) and also increase the thickness of the passive layer formed (Montemor *et al.*, 1998). Owing to these reasonable factors, the passivation of rebar is higher in blended cement concretes than for OPC concrete. From the C_{dl} values, however, the breakdown of passivity could not be detected precisely. For example, the C_{dl} value for the curves shown in Figure 6 is also in the range 60–564 μF , as observed in the passive state, and thus is not

Table 5. Comparison of C_{dl} values with time in 40 MPa concrete (passive condition)

Grade/type of cement	0% chloride				0.5% chloride				1% chloride			
	C_{dl} : $\mu\text{F}/\text{cm}^2$											
	Exposure period: days				Exposure period: days				Exposure period: days			
	0	80	267	540	0	80	267	540	0	80	267	540
40 MPa OPC	561	421	387	413	1079	630	42	211	237	272	161	324
40 MPa PPC	61	69	102	206	79	74	70	189	112	403	141	364
40 MPa PSC	61	73	85	15	83	62	67	82	65	58	286	240

Table 6. Comparison of C_{dl} values with time in OPC concrete (active condition)

Grade/type of cement	0% chloride				0.5% chloride				1% chloride			
	C_{dl} : $\mu\text{F}/\text{cm}^2$											
	Exposure period: days				Exposure period: days				Exposure period: days			
	267	540	1135	1765	267	540	1135	1765	267	540	1135	1765
20 MPa OPC	1107	468	12 718	–	7002	–	–	–	2195	1321	9391	13 434
30 MPa OPC	1379	1386	32 500	1073	1847	3418	7829	49 220	3378	11 275	1477	10 143

able to indicate the state of transition from passivation to initiation of corrosion.

Active condition of the rebar. From Table 6, it can be seen that after 267 days of exposure in both 20 and 30 MPa OPC concretes, the values are greater than 1000 μF right from the initial stage, which indicates severe corrosion of the rebar. Similar values have been reported by others on rough or pre-rusted rebar surfaces (Dawson, 1983; Sagues, 1993).

Polarisation resistance (R_p)

Figure 10 compares the R_p of the rebar at three stages of the corrosion process in 20 MPa concrete. When the rebar is in the passive state, the R_p value of the rebar is greater than 250 $\text{k}\Omega \text{ cm}^2$, and the value falls to less than 230 $\text{k}\Omega \text{ cm}^2$ when corrosion initiates on the rebar. The value decreases to a very low value of less than 14 $\text{k}\Omega \text{ cm}^2$ when corrosion spreads uniformly on the rebar surface. In the case of PPC and PSC concrete, the R_p values are a minimum of three times higher than that of OPC concrete at each stage of the corrosion process. A similar trend is also observed in 30 and 40 MPa concretes.

Phase angle

As in the case of the R_p values, the decrease of the maximum absolute value of phase angle of the rebar has been used to describe the degree of surface corrosion of steel (Mansfeld and Shih, 1988; Mansfeld *et al.*, 1987, 1989; Shih and Mansfeld, 1989). The de-

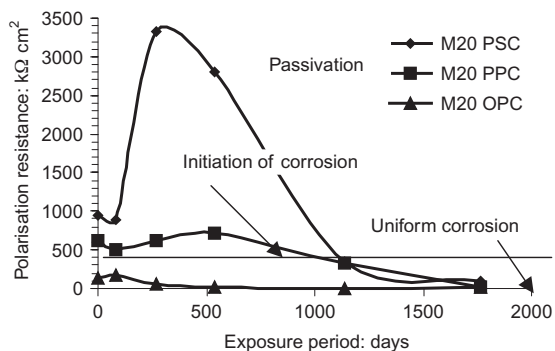


Figure 10. R_p values at three stages of the corrosion process of rebar in 20 MPa concrete

crease of the absolute phase angle is attributed to the decrease of corrosion resistance of the rebar in concrete in the presence of chloride (Gu *et al.*, 1994). From the Bode plots given in Figures 11 and 12, the maximum phase angle is observed at 10 mHz. The phase angle is at a maximum when the rebar is in the passive state in 40 MPa 0% Cl^- added concrete (Figure 11) and at a minimum when the rebar reaches an active state in 20 MPa 0% Cl^- added concrete (Figure 12).

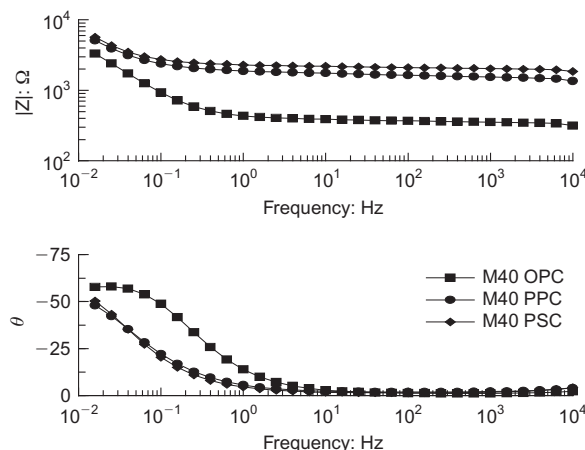


Figure 11. Bode plot of rebar in the passive condition in 40 MPa 0% Cl^- added concrete (80 days)

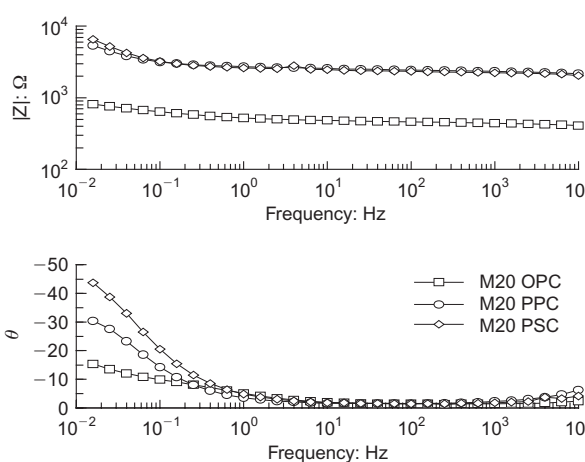


Figure 12. Bode plot of rebar in the active condition in 20 MPa 0% Cl^- added concrete (267 days)

Table 7. Comparison of phase angle

Grade/ type of cement	% of chloride	Phase angle, θ : degrees			
		Exposure period: days			
		267	540	1135	
Active condition (severe corrosion)					
20 MPa OPC	0	16	4	1	
	0.5	5	3	1	
	1	23	3	1	
20 MPa PPC	0	30	28	16	
	0.5	55	8	3	
	1	20	4	5	
20 MPa PSC	0	44	46	6	
	0.5	18	12	4	
	1	17	12	7	
Passive condition					
40 MPa OPC		0	80	267	540
	0	53	58	56	21
	0.5	42	48	56	61
	1	62	64	59	16
40 MPa PPC	0	43	48	41	34
	0.5	51	59	51	39
	1	25	13	13	16
40 MPa PSC	0	42	50	53	47
	0.5	45	46	46	40
	1	34	36	32	28

Table 7 compares the phase angle over time. From the table it can be seen that in 40 MPa concrete initially up to 267 days the values are greater than 30°. In 20 MPa concrete, the rebar attains uniform corrosion, then the values are decreased to less than 20° after 267 days of exposure. The trend is not changed up to the period of 1135 days. Data show that the phase angle can also be used to indicate the depassivation of rebar in chloride contaminated concrete.

Discussion

R_p value versus corrosion rate from weight loss

Figure 13 compares the Nyquist plot of rebar at three stages of corrosion in 30 MPa 0% Cl⁻ added PSC concrete. From the curve it can be seen that the slope of

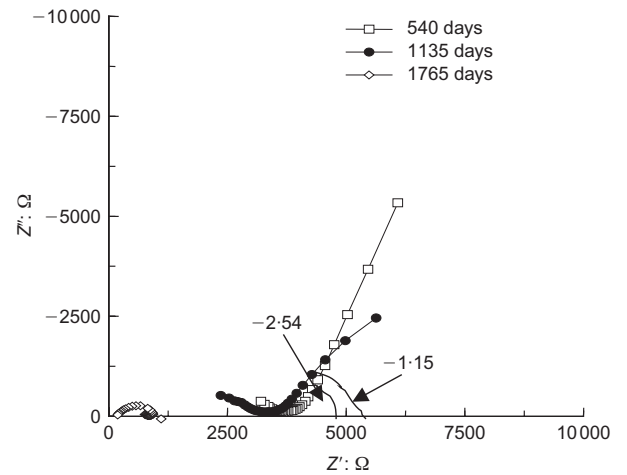


Figure 13. Comparison of Nyquist plots at various stages of corrosion of rebar for 30 MPa 0% Cl⁻ added PSC concrete

the low-frequency arc decreases from -2.54 to -0.20 from the passive to the active state of rebar and it is also shown that the strong decrease of the capacitive part of the impedance response is correlated with the initiation of corrosion. Similarly, from the Bode plot (Figure 14) it is evident that the phase angle is 14°, 23° and 4° at passive state, initiation of corrosion and severe corrosion of rebar, respectively. Table 8 compares the potential and the R_p value of the rebar with the corrosion rate from the weight loss measurement. Until the exposure period of 540 days, when the rebar is in the passive condition, the potential value is -226 mV versus SCE, which is less than -276 mV versus SCE as specified in ASTM C876. As there are no rust spots on the rebar, the R_p value is 4944 kΩ cm² and the corresponding corrosion rate of 0 μm/year from weight loss measurement confirms that the rebar is in the passive state. At the end of 1135 days of exposure when corrosion initiated on the rebar, the potential value of the rebar is -383 mV and the corresponding R_p value is 442 kΩ cm², which is ten times lower than the value obtained for the passive condition. The corrosion rate from weight loss measurement is 1 μm/year. As per the correlation established between the corrosion rate and the degree of corrosion by Martinez *et al.* (2008), the corrosion rate value of 1 μm/year is defined as a low corrosion rate. After 1765 days of exposure, when the rebar attains severe corrosion, the potential value is -284 mV and the R_p value is 32 kΩ cm². The

Table 8. Comparison of R_p, E_{corr} and corrosion rate values in 30 MPa with 1% Cl⁻ added PSC concrete

Days of exposure	Condition of rebar	Slope of low-frequency arc	Potential: mV versus SCE	R _p ; kΩ cm ²	Corrosion rate (from weight loss): μm/y	C _{dl} ; μF/cm ²	Phase angle, θ
540	Passive state	-2.54	-226	4944	0	12	41
1135	Initiation of corrosion	-1.18	-383	442	1	311	23
1765	Severe corrosion	-0.20	-284	32	25.3	1550	4

corresponding corrosion rate from the weight loss measurement is 25.3 $\mu\text{m}/\text{year}$, which is defined as a high corrosion rate. Khatri *et al.* (2004) also reported the similar observation that if the R_p value is in the range 10–60 $\text{k}\Omega \text{ cm}^2$ then there is a significant amount of corrosion on the rebar. It is sometimes difficult to establish a boundary between the state of activity and concentration polarisation (possibly attributable to chloride or oxygen) only on potential values. In such a situation, the evolution of impedance spectra can be useful in the determination of the state of the rebar.

Role of blended cements with respect to time to initiation of corrosion of the rebar. The time at which the rebar attained an R_p value of $\leq 230 \text{ k}\Omega \text{ cm}^2$ has been taken as time to initiation of corrosion ($T_{i,Rp}$). Table 9 compares the T_i from the R_p value with the T_i from the potential measurement ($T_{i,p}$). T_i predicted by $T_{i,p}$ is lower than that of $T_{i,Rp}$ in most of the cases, except that of 20 and 30 MPa OPC concretes. The accuracy of $T_{i,Rp}$ was checked by measuring the corrosion rate at the end of $T_{i,Rp}$ and the values are given in Table 9. The values are $\geq 1 \mu\text{m}/\text{year}$ and are defined as a low corrosion rate, indicating that the corrosion initiated on the rebar. The presence of chloride and moisture movement in the cover concrete influences the measured potential values and this may cause a greater shift in potential in the negative direction than the actual potential value of the rebar; because of this T_i was underestimated by $T_{i,p}$. Khatri *et al.* (2004) also reported that the polarisation resistance is a much more useful and reliable technique in service life evaluation than the half-cell potential. From the table it is also observed that T_i is delayed in PPC and PSC concretes. T_i in PPC and PSC concretes is 15 times higher than that of OPC concrete for 20 MPa; 11 and 14 times higher for 30 MPa; and three times higher for 40 MPa concrete respectively. The data emphasise that the additional calcium hydrates present in the blended cements (Vedalakshmi *et al.*, 2003) increase the tortuosity of the concrete and reduce the chloride diffusivity. This means that the time taken to the occurrence of depassivation

Table 9. Time to initiation of corrosion: OPC versus blended cements

Grade/type of cement	$T_{i,Rp}$: days	$T_{i,p}$: days	Corrosion rate from weight loss method at the end of $T_{i,Rp}$: $\mu\text{m}/\text{year}$
20 MPa OPC	80	151	2.6
20 MPa PPC	1179	508	0
20 MPa PSC	1186	1158	1
30 MPa OPC	102	271	1.28
30 MPa PPC	1135	1158	4.5
30 MPa PSC	1387	1158	1
40 MPa OPC	540	508	1
40 MPa PPC	>1765	>1765	1
40 MPa PSC	1765	1158	1.5

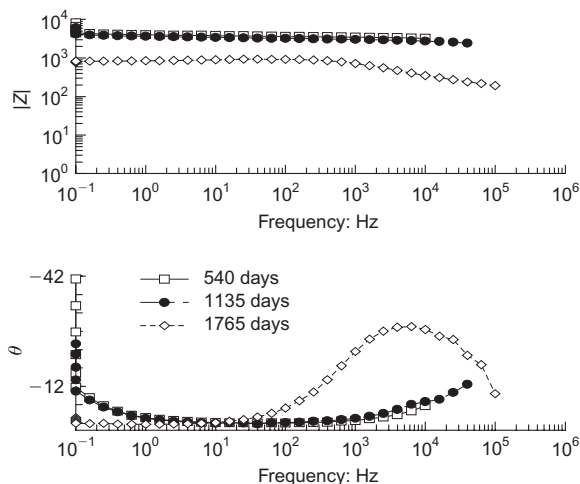


Figure 14. Comparison of Bode plots at various stages of corrosion of rebar for 30 MPa 0% Cl^- added PSC concrete

has been increased considerably in blended cements concrete. In addition to this, the aluminium oxide (Al_2O_3) content of PPC and PSC is 9–11%, which is twice as high as the value for the OPC. The chloride ion binding capacity determined by the standard method (Vogel, 1974) in 1% chloride contaminated concrete is given in Figure 15. From the figure it is clearly evident that, compared to OPC concrete, the chloride ion binding capacity is greater in PPC and PSC concrete in all the three grades of concrete. Higher aluminium oxide content binds a greater amount of chlorides (Dhir *et al.*, 1996; Pruckner, 2001) and a larger number of chloride ions were trapped in the interlayer of additional calcium silicate hydrates formed in the concrete matrix. The above factors contributed to reducing the availability of free chlorides near the rebar level and thus delayed the initiation of corrosion of rebar in blended cement concretes.

Conclusions

- (a) From the EIS spectra, the change in the slope of the low-frequency arc gives the status of the rebar more distinctly than potential measurement. If the slope is greater than -1 , the rebar exhibits purely capacitive behaviour and this denotes it is in the

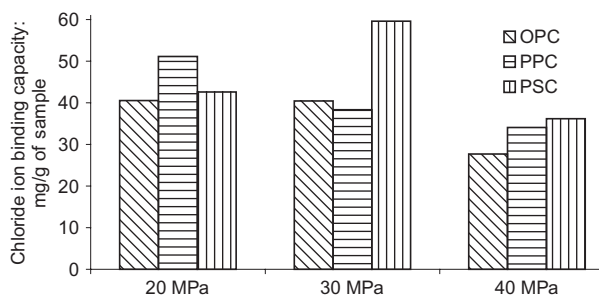


Figure 15. Comparison of bound chloride in 1% chloride-contaminated concrete

perfect passive condition. The rebar in PPC and PSC concretes (0% Cl^- added) has a slope greater than -2 , confirming that the passivation of the rebar is higher than that of OPC concrete.

- (b) If the slope is equal to -1 , the rebar is under mixed kinetic and diffusion control. If the diffusion species are chloride and oxygen then they initiate the corrosion on the rebar. Depending on the rate of diffusion of chloride and the availability of hydroxyl ions, the time taken to initiation of corrosion (T_i) is delayed. Compared to OPC concrete, in PPC and PSC concrete, T_i is delayed by a minimum factor of $\times 10$ in 20 and 30 MPa concretes and $\times 3$ in 40 MPa concrete respectively.
- (c) If the slope is less than -1 , the rebar is under charge transfer control and, depending on the rate of charge transfer, the corrosion spreads uniformly throughout the rebar and attains the severe corrosion state.
- (d) The increase in double layer capacitance $> 500 \mu\text{F}/\text{cm}^2$ indicates a higher adsorption of chloride at the steel–concrete interface. If the value is $> 1000 \mu\text{F}/\text{cm}^2$, then this indicates severe corrosion on the rebar. Under the perfect passive condition, the values are less than $100 \mu\text{F}/\text{cm}^2$. Compared with OPC concrete and PPC concrete, the rebar in PSC concrete shows C_{dl} values that are less than $100 \mu\text{F}/\text{cm}^2$ and maintains the passive condition up to the period of 540 days in the presence of 0.5% chloride.
- (e) R_p values from the Nyquist plot can predict the state of transition from the passive condition to initiation of corrosion quantitatively. If the R_p value is $< 230 \text{ k}\Omega \text{ cm}^2$ then this indicates the initiation of corrosion. In this state, depending on the w/c ratio of the concrete, the type of cement used and the availability of alkalinity, and chloride at the steel–concrete interface, the R_p value varies from 60 to $230 \text{ k}\Omega \text{ cm}^2$. When the rebar attains the severe corrosion condition, the R_p value is $< 14 \text{ k}\Omega \text{ cm}^2$, which causes cracks on the concrete surface. Under the perfect passive state, the R_p value is greater than $250 \text{ k}\Omega \text{ cm}^2$. At each stage of the corrosion processes, the R_p value of the rebar in PPC and PSC concrete is three times (as a minimum) higher than that of OPC concrete in all the three concretes studied.

References

- Andrade C, Alonso C and Molina FG (1993) Cover cracking as a function of bar corrosion Part I: Experimental test. *Materials and Structures* **26(8)**: 453–464.
- Andrade C, Alonso A and Sarria J (2002) Corrosion rate evolution in concrete structures exposed to the atmospheres. *Cement and Concrete Composites* **24(1)**: 55–64.
- Andrade C, Blanco VM, Collazo A, Keddani A, Novoa MR and Takeniuti H (1999) Cement paste hardening process studied by impedance spectroscopy. *Electrochimica Acta* **44(24)**: 4313–4318.
- Arup H (1983) The mechanism of the protection of steel by concrete. In *Corrosion of Reinforcement in Concrete Construction* (Crane AP (ed.)). Ellis Horwood, UK, pp. 151–157.
- Arup H and Sorenson B (1992) A new embeddable reference electrode for use in concrete. *Proceedings of Corrosion/92, NACE, Houston, TX*, Paper No. 208.
- ASTM (American Society for Testing and Materials) (2001a) *Standard Test Method for Half-cell Potentials of Uncoated Reinforcing Steel in Concrete*. ASTM International, West Conshohocken, PA, ASTM C876-91, Vol. 04.02, pp. 452–457.
- ASTM (American Society for Testing and Materials) (2001b) *Standard Practice for the Preparation of Substitute Ocean Water*. ASTM International, West Conshohocken, PA, ASTM-D1141-98, Vol. 11.02.
- ASTM (American Society for Testing and Materials) (2001c) *Standard Practice for Preparing Cleaning and Evaluating Corrosion Test Specimens*. ASTM International, West Conshohocken, PA, ASTM G1-03, Vol. 04.02, pp. 9–14.
- Bennett JE and Amitchell T (1992) Reference electrodes for use with reinforced concrete structures. *Proceedings of Corrosion/92, NACE, Houston, TX*, Paper No. 191.
- BIS (Bureau of Indian Standards) (1985) *Specification for High Strength Deformed Steel Bars and Wires for Concrete Reinforcement*. BIS, New Delhi, India, BIS 1786.
- BIS (Bureau of Indian Standards) (1989a) *Specification for 43 Grade Ordinary Portland Cement*. BIS, New Delhi, India, BIS 8112.
- BIS (Bureau of Indian Standards) (1989b) *Specification for Portland Slag Cement*. BIS, New Delhi, India, BIS 455.
- BIS (Bureau of Indian Standards) (1991) *Specification for Portland Pozzolana Cement (Fly Ash Based)*. BIS, New Delhi, India, BIS 1489 (Part 1).
- Bohnke CI, Bohnke O and Vuillemin B (1993) Constant angle behaviour of SnO_2/WO_3 thin film electrodes in anhydrous LiClO_4 -propylene carbonate electrolyte. *Electrochimica Acta* **38(14)**: 1935–1940.
- Bulu P and Bhattacharjee B (2009) Performance evaluation of rebar in chloride contaminated concrete by corrosion rate. *Construction and Building Materials* **23(6)**: 2346–2356.
- Dawson J (1983) Corrosion monitoring of steel in concrete. In *Corrosion of Reinforcement in Concrete Construction* (Crane AP (ed.)). The Society of Chemical Industry, Ellis Horwood, Chichester, pp. 175–191.
- Dhir RK, Ei-Mohr MAK and Dyer TD (1996) Chloride binding in GGBS concrete. *Cement and Concrete Research* **26(12)**: 1767–1773.
- Dolli H, Muralitharan VS and Rengaswamy NSAP (2003) Reliability evaluation of embeddable reference electrode for use in reinforced concrete structures. *Bulletin of Electrochemistry* **19(1)**: 212–217.
- Feliu S, Gonzalez JA, Andrade MC and Feliu V (1989) Determining polarization resistance in reinforced concrete slab. *Corrosion Science* **29(1)**: 105–113.
- Flis J, Sabol S, Pickering HW, Asseo-Asare K and Caddy PD (1993) Electrochemical measurements on concrete bridges for evaluation of reinforcement corrosion rates. *Corrosion* **49(7)**: 601–613.
- Florr LL and Keith WT (1965) Potential survey method to detect corrosion of prestressed concrete tanks. *Materials Protection* **4(11)**: 49–52.
- Glass GK and Buenfield NR (1999) Differential acid neutralization analysis. *Cement and Concrete Research* **29(10)**: 1681–1684.
- Glass GK, Reddy B and Buenfeld NR (2000) The participation of bound chloride in passive film breakdown on steel in concrete. *Corrosion Science* **42(11)**: 2013–2021.
- Gonzalez JA, Miranda JM and Feliu S (2004) Consideration on reproducibility of potential and corrosion rate measurements in reinforced concrete. *Corrosion Science* **46(10)**: 2467–2485.
- Grantham MG and Broomfield J (1997) The use of linear polarization corrosion rate measurements in aiding rehabilitation options for the deck slabs of a reinforced concrete under car park. *Construction and Building Materials* **11(4)**: 215–224.

- Grimes WD, Hartt WH and Turner DH (1979) Cracking of concrete in seawater due to embedded metal corrosion. *Corrosion* **35(7)**: 309–316.
- Gu P, Ellite S, Hristora R *et al.* (1997) A study of corrosion inhibitor performance in chloride contaminated concrete by electrochemical impedance spectroscopy. *ACI Materials Journal* **94(5)**: 385–395.
- Gu P, Yan F, Xie P and Beaudoin JJ (1994) Characterization of surface corrosion of reinforcing steel in cement paste by low frequency impedance spectroscopy. *Cement and Concrete Research* **24(2)**: 231–242.
- Ismail M and Ohtsu M (2006) Corrosion rate of ordinary and high performance concrete subjected to chloride attack by AC impedance spectroscopy. *Construction and Building Materials* **20(7)**: 458–469.
- John DG, Searson PC and Dawson JL (1981) Use of AC impedance technique: studies on steel in concrete in immersed conditions. *British Corrosion Journal* **16(2)**: 102–106.
- Jovic VD and Jovic BM (2003) EIS and differential capacitance measurements onto single crystal faces in different solutions: Part 1: Ag(III) in 0.01M NaCl. *Journal of Electroanalytical Chemistry* **541**: 1–5.
- Khatri RP, Sirivivatnanon V and Heeley P (2004) Critical polarization resistance in service life determination. *Cement and Concrete Research* **34(5)**: 829–837.
- Lawa DW, Cairns J, Millard SG and Bungey JH (2004) Measurement of loss of steel from reinforcing bars in concrete using linear polarization resistance measurements. *Independent Nondestructive Testing and Evaluation International* **37(5)**: 381–388.
- Mansfeld F and Shih H (1988) Detection of pitting with electrochemical impedance spectroscopy. *Journal of Applied Electrochemistry* **13(4)**: 1171–1172.
- Mansfeld F, Lin S, Kim S and Shih H (1987) Pitting and surface modification of SiC/Al. *Corrosion Science* **27(9)**: 997–1000.
- Mansfeld F, Lin S, Kim S and Shih H (1989) Corrosion protection of Al alloys and Al-based metal matrix composites by chemical passivation. *Corrosion* **4(8)**: 615–630.
- Martinez I, Andrade C, Rebolledo N *et al.* (2008) Corrosion characterization of reinforced concrete slabs with different devices. *Corrosion* **64(2)**: 107–123.
- Montemor MF, Simoes AMP and Ferreira MGS (1998) Analytical characterization of the passive film formed on steel in solutions simulating the concrete interstitial electrolyte. *Corrosion* **54(5)**: 347–353.
- Montemor MF, Simoes AMP and Salta MM (2000) Effect of fly ash on concrete reinforcement corrosion studied by EIS. *Cement and Concrete Composites* **22(3)**: 175–185.
- Monticelli C, Frignani A and TrabANELLI A (2000) A study on corrosion inhibitors for concrete application. *Cement and Concrete Research* **30(4)**: 635–642.
- Morris W, Vico A, Vazquez M and De Sanchez SR (2002) Corrosion of reinforcing steel evaluated by means of concrete resistivity measurements. *Corrosion Science* **44(1)**: 81–99.
- Pruckner F (2001) *Corrosion and Protection of Reinforcement in Concrete: Measurements and Interpretations*. PhD thesis, Faculty of Natural Sciences and Mathematics, University of Vienna, pp. 132–133.
- Rammelt U and Reinhard G (1995) Impedance analysis of conversion layers on iron. *Electrochimica Acta* **40(4)**: 505–517.
- Rengaswamy NS, Balasubramaniyan TM, Srinivasan S, Mahadeviyer YM and Suresh Babu RH (1987) Corrosion survey of bridges. *The Indian Concrete Journal* **61(6)**: 147–160.
- Sagoe-Crentsil KK and Glasser FP (1989) Steel in concrete. Part I: A review of the electrochemical and thermodynamic aspects. *Magazine of Concrete Research* **41(149)**: 205–212.
- Sagues AA (1993) Corrosion measurement techniques for steel in concrete. *Proceedings of Corrosion/93, NACE, Houston, TX*, Paper No. 353.
- Sagues AA, Kranc SC and Moreno EI (1995) The time–domain response of a corroding system with constant phase angle interfacial component application to steel in concrete. *Corrosion Science* **37(7)**: 1097–1113.
- Sergi G and Glass GK (2000) A method of ranking the aggressive nature of chloride contaminated concrete. *Corrosion Science* **42(12)**: 2043–2049.
- Shih H and Mansfeld F (1989) A fitting procedure for impedance spectra obtained for cases of localized corrosion. *Corrosion* **4(8)**: 610–614.
- Stratfull RF (1957) The corrosion of steel in reinforced concrete bridges. *Corrosion* **13(3)**: 43–48.
- Vedalakshmi R, Sundararaj A, Srinivasan S and Ganesh Babu K (2003) Quantification on hydrated cement products of blended cements in low and medium strength concrete using TG and DTA technique. *Thermochimica Acta* **407(1–2)**: 49–60.
- Videm K (1998) The reliability of electrochemical techniques for assessing corrosion of steel in concrete. *Proceedings of Corrosion/98, NACE, Houston, TX*, Paper No. 749.
- Villela T, Souza A and Abdel-Rehim H (2004) Silver/silver chloride and mercury/mercurous sulfate standards electrodes confiability. *Corrosion* **60(4)**: 342–345.
- Vogel AI (1974) *A Text Book of Quantitative Inorganic Analysis Including Elementary Instrumental Analysis*. Longman, London, pp. 72–81.
- Wenger F and Galland J (1990) Analysis of local corrosion of large metallic structures or reinforced concrete structures by electrochemical impedance spectroscopy. *Electrochimica Acta* **35(10)**: 1573–1578.
- Zivica V (2001) Possibility of improvement of potentiodynamic method for monitoring corrosion rate of steel reinforcement in concrete. *Bulletin of Material Science* **24(5)**: 555–558.

Discussion contributions on this paper should reach the editor by 1 September 2010